wind

MDPI

Article

Wind Characteristics and Energy Evaluation at Nasiriya International Airport, Iraq

Firas A. Hadi [1,*], Sarmad Jasim Hasan [2], Qutaiba Mazin Abdulmajeed [3], Rawnak A. Abdulwahab [4] and Khattab Al-Khafaji [5,*]

[1] Department of Renewable Energy Science, College of Energy and Environmental Sciences, Al-Karkh University of Science, Baghdad 10081, Iraq
[2] Wind Department of Energy, Al-Nahrain Research Center for Renewable Energy, Al-Nahrain University, Baghdad 10070, Iraq; sarmad_jh@nahrainuniv.edu.iq
[3] Electronic and Communications Engineering Department, College of Engineering, Al-Nahrain University, Baghdad 10070, Iraq; qutaiba.mazin.elc@nahrainuniv.edu.iq
[4] Remote Sensing Research Department, Space Research and Technology Center, Scientific Research Commission, Baghdad 10070, Iraq; drrawnakadel@mohesr.edu.iq
[5] Department of Environmental Science, College of Energy and Environmental Sciences, Al-Karkh University of Science, Baghdad 10081, Iraq
* Correspondence: firas.a.hadi@kus.edu.iq (F.A.H.); k.a.alkhafaji@gmail.com (K.A.-K.)

Abstract

In order to reduce aviation's negative environmental effects and support international efforts to battle climate change, the International Civil Aviation Organization (ICAO) seeks to cut greenhouse gas (GHG) emissions. About 2–3% of the world's CO_2 emissions come from aviation, and at high altitudes, the fraction of other GHGs that significantly alter the atmosphere is considerably greater. In this study, hourly wind speed data at 100 m height from ECMWF's fifth-generation reanalysis (ERA-5) were used over a period of 40 years (1985–2025). Hourly assessments of wind speeds at 40 m and 80 m heights are conducted in ERA-5, with biases at specific ground locations rectified via the Global Wind Atlas (GWA). This research estimates and analyzes many factors, including Weibull statistical parameters, daily and monthly wind speed variations, cumulative distribution function (CDF), and atmospheric turbulence intensity. The energy generation from several wind turbine types at different elevations was assessed. The findings indicate that the examined location revealed fair potential for the construction of large-capacity wind energy units at heights equal to or above 80 m. Turbines that are less than 50 m tall are spread out at least 10 km around the airport runway. While turbines that are less than 150 m tall are spread out at least 15 km away from the airport runway.

Keywords: wind energy; Weibull; airports; wind turbine; aviation; carbon dioxide; turbulence intensity

Check for updates

Academic Editor: Adrian Ilinca

Received: 27 March 2026
Revised: 25 May 2026
Accepted: 22 June 2026
Published: 6 July 2026

Copyright: © 2026 by the authors. Licensee MDPI, Basel, Switzerland. This article is an open access article distributed under the terms and conditions of the Creative Commons Attribution (CC BY) license.

1. Introduction

Aviation-related GHG emissions are a contributing factor to global warming, which intensifies extreme weather events and disturbs ecosystems. To support the objectives of the Paris Agreement, ICAO seeks to control the rise in global temperatures. As a significant worldwide business, aviation has an obligation to minimize its negative environmental effects. Reducing GHG emissions contributes to the sector's sustainable expansion while protecting the environment [1]. By establishing international aviation standards, ICAO makes sure that nations and airlines all around the globe follow uniform laws designed to lower GHG

emissions. One of the main tactics the ICAO advocates in its attempts to make aviation more sustainable is the use of renewable energy to lower GHG emissions. Compared to fossil fuels, which are the main cause of CO_2 and other GHG emissions in aviation, renewable energy provides a greener option. Wind energy is one of the important sources of renewable energy, which is considered the second most widespread main source in the world after solar energy. Research on creating an environmentally friendly, sustainable airport with little effect has been carried out by several researchers worldwide [2].

As the 21st century began and the world started to want more renewable energy, research started to concentrate on particular uses and improvements. During this time, more advanced optimization approaches for renewable energy systems began to appear. Ortega Alba and Manana (2016) conducted an extensive assessment of airport energy studies, highlighting that the fast expansion of aviation activities has resulted in heightened energy consumption, therefore escalating prices and environmental repercussions. During this time, there were additional studies done on Rome's Leonardo da Vinci International Airport [3]. de Rubeis et al. (2016) suggested an electrical energy optimization platform that looked at power, heat, and fuel use across many years [4]. Cuadra et al. (2019) developed a methodology to study the impact of air traffic rights on the establishment of wind farms near airports and conducted a comprehensive study of obstruction roofs and related legislation [5]. These rights have significantly influenced the site selection and construction of wind farms. Santa et al. (2020) presented a "green airport model" derived from social and ecological management frameworks, leveraging recent legislation that encourages sustainable development projects [6]. Xiang et al. (2021) studied the technical and economic advantages of integrating hydrogen supply, auxiliary power units, and solar energy into airport microgrids to achieve net-zero emissions in airport operations [7].

Goh et al. (2024) devised an adaptive energy management strategy for Copenhagen Airport, illustrating the feasibility of sustaining a reliable and low-carbon energy supply [8]. A study conducted by Al-Zain et al. (2025) demonstrated that airports exhibit variations in the maturity levels of their energy and sustainability strategies from an institutional standpoint. While certain entities adopt comprehensive environmental management systems, others are satisfied with the implementation of isolated initiatives. This article analyzes wind data at Nasriya Airport to evaluate and assess wind turbine output energy production from different heights and wind turbines at this location [9].

By combining wind characteristics analysis, Weibull distribution modeling, turbulence intensity assessment, and wind turbine performance at various hub heights, the current study offers a thorough evaluation of the wind energy potential at Nasiriyah Airport, Iraq. The integration of wind resource assessment with airport operational considerations, including the assessment of appropriate turbine placement distances in relation to runway safety requirements, is one of the primary innovations of this work. Additionally, in order to determine appropriate configurations for energy generation in the study area, the study evaluates the performance of several wind turbines under local wind conditions. But there are a few restrictions that need to be noted. Furthermore, before considering large-scale wind energy development close to the airport, more aviation safety investigations and on-site measurements are advised.

2. Research Objective

ICAO seeks to reduce GHG emissions. Aviation accounts for approximately 2–3% of global carbon dioxide emissions. The study's specific objectives are to assess the wind energy potential at Nasiriya Airport to help determine if green infrastructure at Iraqi public airport is possible. The results will also give investors, airport management, and legislators important information about the possible advantages and difficulties of putting wind farms in airports.

3. Materials and Methods

3.1. Description of the Studied Site

In Nasiriya, the dominant northwesterly winds are prevalent in both winter and summer, delivering dry air that may reduce temperatures in the cooler months and intensify dust storms and wind disturbances over the area. Climatological investigations indicate that northwesterly and westerly winds are predominant at Nasiriya's weather stations.

Nasiriya Airport is located in Nasiriya governorate at Lat. 30.933582°, Lon. 46.087617° and 7 m above sea level. The governorate is about 360 km south of Baghdad (the capital of Iraq) and 18 km from the city center. It has moderate and seasonally consistent northwesterly winds, with mean wind speeds suitable for small-to-medium-scale wind power production at hub heights of around 50 m. The level and open landscape around the airport reduces surface roughness and turbulence, hence improving turbine efficiency. The presence of extensive safety buffer zones facilitates turbine construction without compromising aircraft safety or airport operations. On-site wind power may partly mitigate the airport's constant energy demand and reduce dependence on the national grid and fossil fuel-based backup systems. This results in reduced operating expenses and enhanced environmental performance at the airport. Figure 1 illustrates the geographical position of Nasiriyah city in Iraq along with its administrative boundaries. Figure 2 illustrates the geographical position of Nasiriyah Airport, the focus of this study. Figure 3 illustrates the geographical location and schematic layout of Nasiriya Airport in Nasiriyah Governorate, Iraq.



Figure 1. Location of the governorate that includes the airport [10].



Figure 2. Position of the studied site in Iraq (Red Balloon) [10].

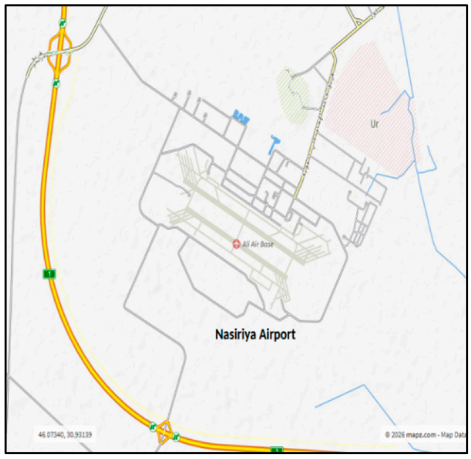


Figure 3. Map of Nasiriya Airport [10].

Figure 4 represents the procedure for correcting ERA-5 wind speed bias using the GWA for Nasiriya Airport at a height of 100 m, including scaling correction and Weibull parameter modification.

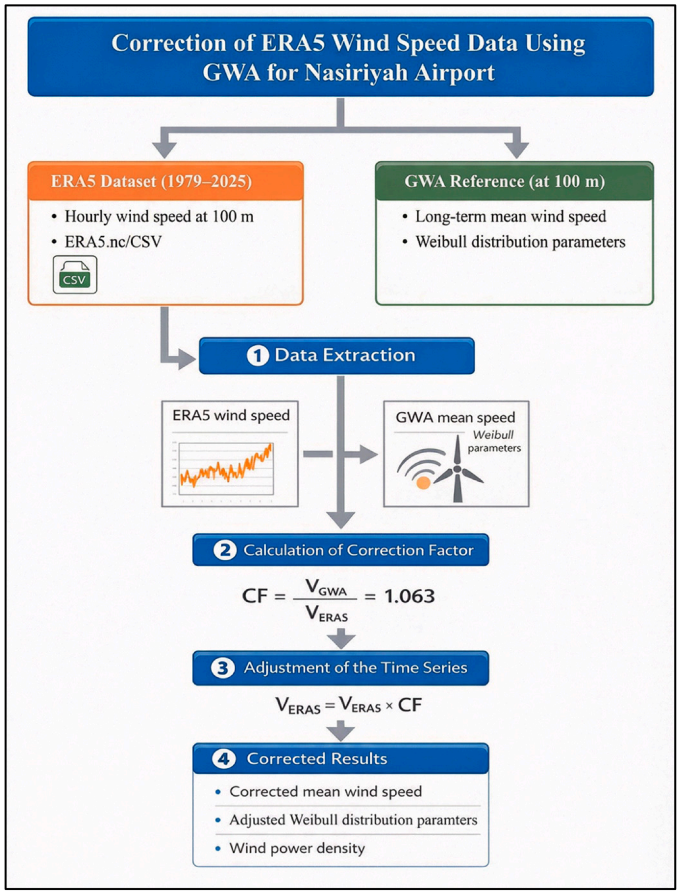


Figure 4. ERA-5 data correction using the GWA.

ERA-5 wind speed data from 1985 to 2025 at Nasiriyah Airport were used to identify wind energy resources. Wind speed frequency distributions were analyzed using the Weibull distribution. Wind power and energy density were derived, and the energy productivity of turbines with different characteristics, specifications, and heights was evaluated assuming their presence at the airport site. Specifications were selected to be

suitable for the airport site and not in violation of ICAO regulations. Figure 5 illustrates the methodological framework of the research.

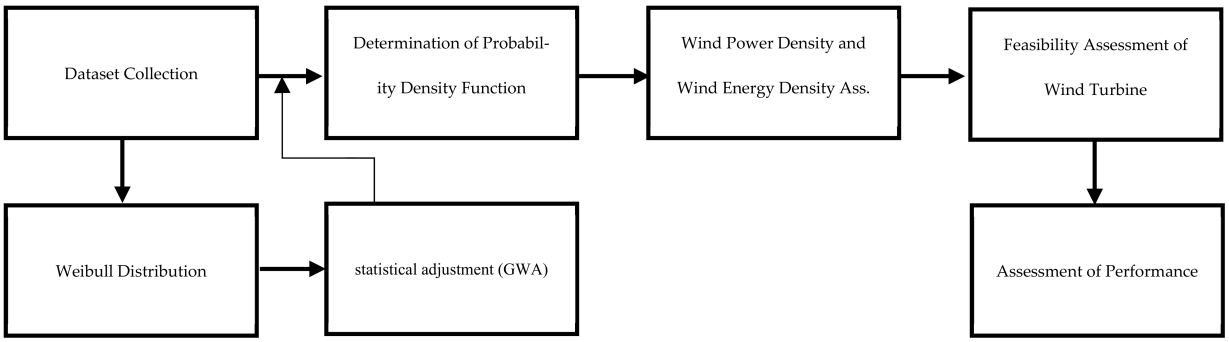


Figure 5. Schematic representation of the overall structure of the proposed framework.

3.2. Dataset Collection

The European Reanalysis datasets, known as ERA-5, are generated by the European Center for Medium-Range Weather Forecasts (ECMWF). ERA reanalysis datasets have been extensively utilized, assessed, and employed in this study for wind energy evaluation. They provide the highest spatial resolution among global reanalysis datasets ($0.25^\circ \times 0.25^\circ$, approximately 28×28 km), with a temporal coverage spanning 40 years (1985–2025) at an hourly resolution at 100 m elevation. Hourly ERA-5 wind speed data at 100 m were statistically adjusted utilizing the Global Wind Atlas (GWA) as a high-resolution spatial reference. A bias correction factor was calculated based on the ratio of long-term mean wind velocities, with Weibull distribution parameters adjusted proportionately. This hybrid Weibull–scaling methodology markedly enhances the depiction of local wind features at Nasiriya Airport.

4. Experimental Approach

4.1. Weibull Statistical Distribution

Statistical procedures may be used to quantify a location's wind power. For wind energy systems, a number of probability functions may be applied to characterize the statistical distribution of wind speed. The Weibull distribution is the most effective, exhibiting an adequate degree of accuracy. This tool facilitates the rapid calculation of the mean yearly output of a certain wind turbine. The probability density function for wind speed can be defined according to [11]:

$$f(v) = \left(\frac{k}{c}\right)\left(\frac{v}{c}\right)^{k-1} exp\left[-\left(\frac{v}{c}\right)^{k}\right] \quad \text{Note}: \; k > 0, \; v > 0, \; c > 1 \tag{1}$$

where v wind speed, both k and c are Weibull parameters, they are the so-called shape factor (k) and scale factor (c m/s), respectively.

The Weibull parameters k and c describe the wind potential of the studied location. The scale parameter c denotes the intensity of wind at a specific location, while the shape parameter k reflects the concentration of wind speeds around a particular value [12].

4.2. Wind Power Density (WPD)

Wind Power potential Density (WPD) represents extractable wind power relative to a square meter of area (rotor swept area) and is a fundamental indicator for evaluating

wind resources potential among different locations and turbine types. WPD is directly proportional to air density and wind speed cubed, typically expressed as [13,14]:

$$W_p = \frac{1}{2n}\sum_{i=1}^{n}\rho v_i^3 \tag{2}$$

where n is the number of recordings in the mean period, ρ is the density of the air, and v_i^3 is the cube of the ith wind speed value.

Now, if A is the blade sweep area, U is the average wind speed, then wind power density in terms of the Weibull distribution function is given by [15,16]:

$$\frac{P}{A} = \int_0^\infty \frac{1}{2}\rho U^3 f(U)d(U) = \frac{1}{2}\rho c^3 \Gamma\left(1+\frac{3}{k}\right) \tag{3}$$

where is the gamma function of (x) equal to:

$$\Gamma(x) = \int_0^\infty e^{-u}u^{x-1}du \tag{4}$$

4.3. Cumulative Distribution Function CDF

The cumulative frequency distribution function $f(U)$ is another important statistical measure. It shows the chance or time fraction that $U \leq$ a certain U, Equation (5) [17]:

$$f(U) = 1 - \exp\left[-\left(\frac{U}{c}\right)^k\right] \tag{5}$$

4.4. Turbulence Intensity Equation

Rapid disruptions or abnormalities in wind direction, speed, and vertical component are known as wind turbulence. Because high turbulence levels may reduce power production and result in excessive stress on wind turbine components, it is an essential site attribute. The wind speed standard deviation (σ) is the most often used metric of turbulence for siting reasons. Turbulence intensity (TI), which may be computed using Equation (6), is obtained by normalizing the standard deviation value with the mean wind speed (U) [18]:

$$\boldsymbol{TI} = \frac{\boldsymbol{\sigma}}{\boldsymbol{U}} \tag{6}$$

4.5. Vertical Extrapolation

If the altitude at which measurements are made is not at the hub height of a wind turbine, it is necessary to extrapolate the wind speeds to hub height. The methods required for extending the obtainable wind speeds at the hub height of a turbine are described in Equations (7) and (8). Equation (7) represents the basic form of power law wind profile [19]:

$$\boldsymbol{v} = \boldsymbol{v_r}\left(\frac{\boldsymbol{z}}{\boldsymbol{z_r}}\right)^{\boldsymbol{\alpha}} \tag{7}$$

When v denotes wind speed at height z, v_r represents wind speed at a reference height z_r, and α is the wind shear exponent. Consequently, the value of α may be determined by Equation (8) [11]:

$$\boldsymbol{\alpha} = \frac{\boldsymbol{log}\left(\frac{v_r}{v}\right)}{\boldsymbol{log}\left(\frac{z_r}{z}\right)} \tag{8}$$

4.6. Turbulence Intensity Modeling

Turbulence intensity (*TI*) was not quantified directly due to the lack of high-frequency wind speed data at the research location. The ECMWF instead supplied the synthetic *TI* data, which was based on the ERA5 reanalysis mean wind speed. Although ERA5 datasets provide mean wind speeds across time and reflect simulated atmospheric conditions, they lack the short-term variations in wind speed that are necessary for direct turbulence measurement [20]. To overcome this constraint, the reference turbulence model outlined in the International Electrotechnical Commission's (IEC) 61400-1 standard for the design of wind turbines was used. It was assumed that the research location was in a Class A reference turbulence category (I_{ref} = 0.14), which is characteristic of wide terrain and semi-arid conditions. For every 10 min interval, the turbulence intensity was determined by [21,22]:

$$\boldsymbol{TI} = \boldsymbol{I_{ref}}\left(\frac{\mathbf{15}}{\overline{\boldsymbol{v}}}\right)^{\mathbf{0.2}} \tag{9}$$

where the mean wind speed at the given height is represented by $\overline{v}$. In order to conduct turbulence analysis in the wind resource assessment program, the standard deviation of wind speed (σ) was subsequently retrieved from [21,22]:

$$\boldsymbol{\sigma} = \boldsymbol{TI} \times \overline{\boldsymbol{v}} \tag{10}$$

This method allows for the first characterization of turbulence in order to evaluate wind resources and turbine compatibility. It is important to mention that the *TI* values that are obtained are standardized estimates and not based on site-specific observed turbulence. IEC 61400-1 3rd categorizes wind turbine generators based on wind speed characteristics and ambient turbulence conditions. From Table 1, wind speed classification (I, II, or III) is based on the long-term average wind speed (v_{ave}) and the 50-year reference extreme wind speed (v_{ref}), while turbulence subclasses (A, B, and C) are defined by the reference ambient turbulence intensity (TI_{ref}) evaluated at 15 m/s. The comprehensive turbine classification incorporates both criteria (e.g., Class III-A), ensuring sufficient structural integrity and fatigue load resistance under certain wind conditions [23].

Table 1. Wind turbine class and subclass definition [24].

WTG Class	I	II	III
V_{ave} (m/s)	10	8.5	7.5
V_{ref} (m/s)	50	42.5	37.5
A TI_{ref}		0.16	
B TI_{ref}		0.14	
C TI_{ref}		0.12	

A, B and C define turbulence categories. TI_{ref} is the ambient turbulence intensity reference value.

While the IEC 61400-1 framework provides a feasible approach for initial wind resources evaluation, it does not directly consider localized flow effects caused by complex terrain features, aviation infrastructure, and surrounding obstacles. Recently Computational Fluid Dynamics (CDF) techniques have been widely adopted to enhance turbulence analysis by manipulating 3D airflow structure and wake effects surrounding wind turbines. CFD simulations based on Reynolds-Averaged Navier–Stokes (RANS) models, especially those utilizing SST turbulence models, have shown strong capability in evaluating turbulence intensity patterns, wind shear, airflow separation, the wake behavior in wind energy analysis. These methods are highly effective in aviation fields where terminal building, infrastructure, and runway layouts can locally alter boundary layer flow. Hence, while

the current study is based on the conventional IEC turbulence model in the absence of high-frequency observational data, future studies should integrate CFD-based analysis and site-specific measurements to enable a more accurate depiction of turbulence properties and turbine-flow interactions at Nasiriyah airport to improve turbulence analysis [25].

4.7. Wind Turbine Energy Production

The mean power generated by the wind machine, P_W, is determined by the probability distribution, *P(U)*, and the established turbine performance curve, *Pw(U)*, as seen in Equation (11) [26]:

$$\boldsymbol{P_w} = \int_{\mathbf{0}}^{\infty} \boldsymbol{P(U)P(U)dU} \tag{11}$$

Consequently, by summing across *N* bins, the following statement may be employed to get the mean wind machine power [26]:

$$P_w = \sum_{i=1}^{N_B} \frac{1}{2}(U_{i+1} - U_i)(P(U_{i+1})P_w(U_{i+1}) + P(U_i)P_w(U_i)) \tag{12}$$

Equation (12) may be used to determine the mean power output of a wind machine, which can then be used to estimate the total yearly energy harvested by a wind turbine through the operating time period Δt [27]:

$$E_w = P_w \times N \times \Delta t \tag{13}$$

If P_R represents turbine rated power and *CF* denotes the capacity factor, the turbine annual energy production E_I is:

$$E_I = 8760 \times P_R \times CF \tag{14}$$

The *CF* is the mean power production relative to its rated power. The capacity factor is the most accurate metric that reflects the power-generating efficiency [12].

4.8. DistanceHeight Constraints

In this study, hub heights of 40, 80, and 100 m were chosen to reflect typical wind turbine configurations and assess the impact of hub height on wind characteristics and energy production at Nasiriyah Airport. The permitted turbine setback distances shown in Table 2 and airport operational safety restrictions also played a role in the selection of these heights. The 40 m hub height was specifically taken into consideration to evaluate lower-height turbine configurations within shorter permitted setback distances, while the 80 m and 100 m hub heights were examined to look into the possibility of an increase in wind energy production with elevation. A comparative evaluation of turbine performance under both aerodynamic and aviation safety constraints is made possible by this multi-height approach. The height limitations for wind turbines next to Nasiriyah Civil Airport are listed in Table 2.

Table 2. Height restrictions for wind turbines adjacent to the Nasiriya civil airport [28,29].

Proximity to Runway	Allowed Turbine Height
<3 km	Not permitted
3–6 km	≤30–45 m
6–15 km	≤100 m
>15 km	Up to 150–200 m

Heights in Table 2 refer to maximum blade tip height above ground level [30].

5. Results and Discussion

Wind data were extracted from the European Reanalysis (ERA-5), collected over approximately 40 years from 1985 to 2025, at 60 min intervals at a height of 100 m, and analyzed using Windographer version 4 software. Wind data at heights of 80 m and 40 m were estimated using vertical extrapolation in Equation (7).

5.1. Wind Speed Patterns

Figure 6 shows the mean hourly wind speed for each month. Generally, wind speeds are higher in the warmer months (May, Jun., Jul., Aug., Sep.) than in the colder months. The highest mean wind speeds are recorded in July (8.1 m/s, 9 m/s, and 9.4 m/s) at altitudes 40 m, 80 m, and 100 m, 8:00 PM (Figure 7), respectively. The lowest mean wind speeds are recorded in November (5.3 m/s, 5.8 m/s, and 6 m/s) at altitudes of 40 m, 80 m, and 100 m, respectively. Tables 3–5 provide the monthly mean wind speeds, minimum and maximum, standard deviations values, as well as Weibull parameters for Nasiriya Airport at altitudes of 40, 80, and 100 m.

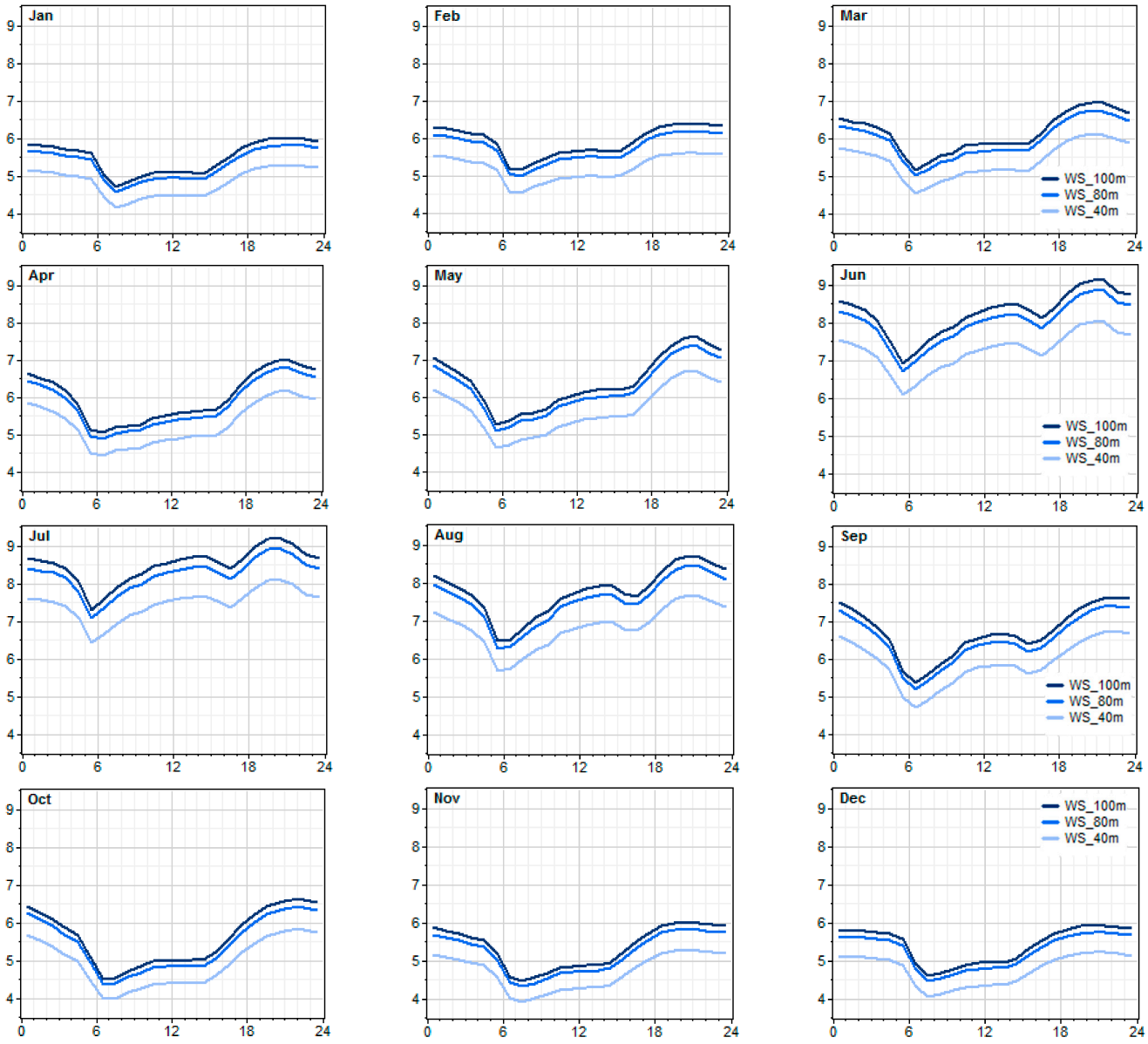


Figure 6. Hourly mean wind speed for whole months.

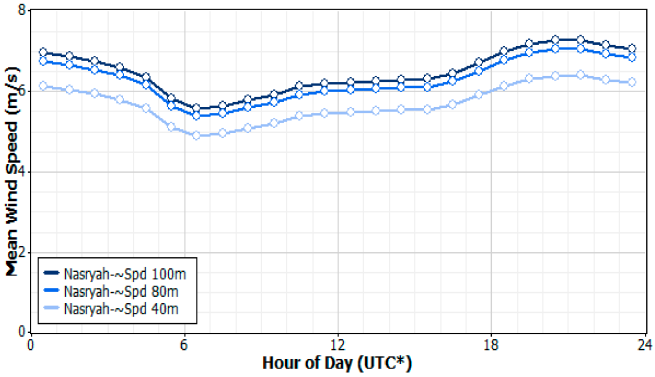


Figure 7. Monthly mean wind speed.

Table 3. Wind speed statistics at 40 m height.

Month	Mean Wind Speed (m/s)	Min	Max	σ (m/s)	k	c (m/s)
Jan	4.841	0.035	16.220	2.296	2.217	5.457
Feb	5.215	0.017	16.097	2.437	2.254	5.879
Mar	5.423	0.080	17.065	2.582	2.206	6.114
Apr	5.293	0.043	17.838	2.524	2.206	5.968
May	5.666	0.043	15.763	2.442	2.483	6.376
Jun	7.278	0.043	15.929	2.623	3.086	8.124
Jul	7.490	0.071	15.437	2.481	3.406	8.319
Aug	6.853	0.035	14.699	2.485	3.070	7.652
Sep	5.917	0.052	14.699	2.410	2.659	6.639
Oct	4.947	0.043	14.364	2.261	2.316	5.572
Nov	4.725	0.026	13.678	2.164	2.306	5.323
Dec	4.781	0.052	13.045	2.244	2.245	5.389
All	5.708	0.017	17.838	2.595	2.331	6.428

Table 4. Wind speed statistics at 80 m height.

Month	Mean Wind Speed (m/s)	Min	Max	σ (m/s)	k	c (m/s)
Jan	5.334	0.039	17.873	2.530	2.217	6.013
Feb	5.746	0.019	17.737	2.686	2.254	6.478
Mar	5.976	0.087	18.803	2.845	2.206	6.737
Apr	5.832	0.048	19.656	2.782	2.206	6.577
May	6.243	0.048	17.369	2.691	2.483	7.025
Jun	8.020	0.048	17.553	2.891	3.086	8.952
Jul	8.254	0.078	17.010	2.733	3.406	9.166
Aug	7.552	0.039	16.196	2.739	3.070	8.431
Sep	6.520	0.058	15.828	2.656	2.659	7.315
Oct	5.451	0.048	15.091	2.491	2.316	6.140
Nov	5.207	0.029	15.072	2.385	2.306	5.865
Dec	5.268	0.058	14.374	2.473	2.245	5.938
All	6.290	0.019	19.656	2.859	2.331	7.083

Figure 7 shows the hourly mean wind speed. This figure indicates the times of day with favorable wind speeds throughout the year. Wind speeds are optimal between 7:00 and 11:00 PM at all elevations, while mean wind speeds are weak between 5:00 and 7:00 AM at all elevations. Therefore, it can be concluded that strong winds often blow during the night at elevations between 40 and 100 m.

Table 5. Wind speed statistics at 100 m height.

Month	Mean Wind Speed (m/s)	Min	Max	σ (m/s)	k	c (m/s)
Jan	5.503	0.040	18.440	2.611	2.217	6.204
Feb	5.929	0.020	18.300	2.771	2.254	6.683
Mar	6.165	0.090	19.400	2.935	2.206	6.951
Apr	6.017	0.050	20.280	2.870	2.206	6.785
May	6.441	0.050	17.920	2.776	2.483	7.248
Jun	8.274	0.050	18.110	2.982	3.086	9.236
Jul	8.516	0.080	17.550	2.820	3.406	9.457
Aug	7.791	0.040	16.710	2.826	3.070	8.699
Sep	6.727	0.060	16.330	2.740	2.659	7.548
Oct	5.624	0.050	15.570	2.570	2.316	6.334
Nov	5.372	0.030	15.550	2.461	2.306	6.051
Dec	5.435	0.060	14.830	2.551	2.245	6.126
All	6.489	0.020	20.280	2.950	2.331	7.308

At 40 m above the ground (Table 3), the greatest mean wind speed reached 7.49 m/s in July, accompanied by a Weibull k of 3.40 and a Weibull c of 8.31 m/s. The peak standard deviation was recorded in June at 2.62 m/s. The monthly mean wind speed varied from 4.7 m/s in November to 7.4 m/s in July (Figure 8). The minimum mean wind speed monthly is around nil, and the highest surpasses 17 m/s in April. It can be noticed that the largest mean wind speed is in June and July, signifying that wind turbines may capture more wind energy at those months. From April to July, the Weibull k parameter increases from 2.20 to 3.40, as seen in Table 3. The Weibull c value fluctuates from 5.45 in January to 8.31 in July.

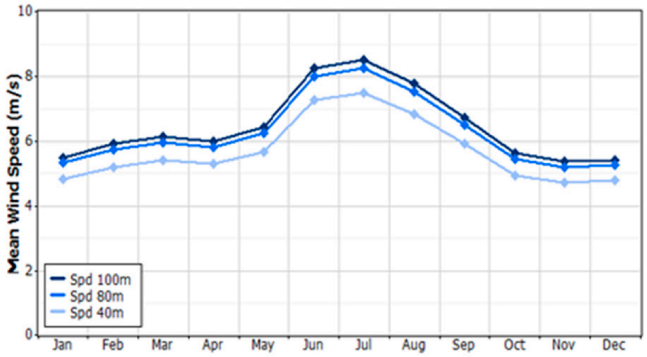


Figure 8. Hourly mean wind speed for the whole year.

In July (Table 4) the greatest mean wind speed reached 8.254 m/s, accompanied by a Weibull k of 3.40 and a Weibull c of 9.16 m/s at an elevation of 80 m. The peak standard deviation was recorded in June, at 2.891 m/s. The monthly mean wind speed varied from 5.20 m/s in Nov to 8.254 m/s in Jul. The minimum mean wind speed monthly is around nil, and the highest surpasses 19 m/s. In June and July, the mean wind speed surpasses 8 m/s, signifying that wind turbines may capture more wind energy. From May and April to July, the Weibull k parameter increases from 2.20 to 3.40. The Weibull c value fluctuates from 5.86 m/s in January to 9.1 m/s in July.

In July (Table 5), the highest mean wind speed was 8.516 m/s with a Weibull k of 3.40 and c of 9.457 m/s at 100 m. June had the highest standard deviation, 2.982 m/s. The mean wind speed varies from 5.3 m/s in Nov to 8.5 m/s in Jul. The monthly mean wind speed ranges from a minimum of 0 to a maximum of 20 m/s. The mean wind speeds over the course of a year are 5.708 m/s, 6.290 m/s, and 6.489 m/s at heights of 40 m, 80 m, and

100 m, respectively. The mean wind speed shows that Nasiriya is a good area to generate wind energy.

Figure 8 shows similar patterns of the monthly mean wind speed at adopted heights based on Tables 3–5. Also, this figure shows that the monthly speeds at 40 m, 80 m, and 100 m heights vary from 4.9 m/s, 5.2 m/s, and 5.4 m/s in November to 7.4 m/s, 8.2 m/s, and 8.5 m/s in July, respectively. Table 3 indicates that at a height of 40 m, wind speeds throughout winter, from December to February, vary from 4.7 to 5.4 m/s. During spring, from March to May, wind speeds vary from 5.2 to 5.6 m/s. During the summer months of June to August, wind speeds vary from 6.8 to 7.4 m/s. In the Autumn months of September to November, wind speeds range from 4.7 to 5.9 m/s. Consequently, the summer season has a greater possibility for wind at Nasiriya Airport. This truth is applicable to the additional heights of 80 m and 100 m (Tables 4 and 5). Wind energy can be used to supplement the electrical power used at the airport, whether for lighting, heating, or cooling. The speed of wind for the cold and warm seasons is shown in Table 6 for Nasiriya Airport at three elevations. The mean wind speed during the warm season exceeds that during the cold season at 40 m, 80 m, and 100 m.

Table 6. Seasonal wind for Nasiriya Airport at 40 m, 80 m, and 100 m heights.

Height (m)	Coled Season (m/s)	Warm Season (m/s)
40	5.06	6.02
80	5.58	6.63
100	5.75	6.84

5.2. Wind Speed Distribution

Using the Weibull probability function, frequency distributions of wind speeds have been computed. Graphs in Figures 9–11 demonstrate that the actual distribution data is best represented by the Weibull distribution. Figures 9–11 show Weibull *k* and *c* statistical parameters of the Weibull probability distribution function at heights of 40 m, 80 m, and 100 m, respectively.

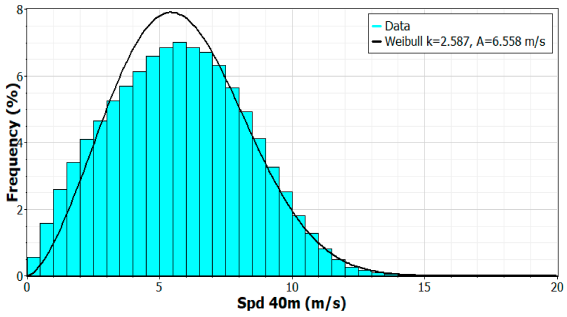


Figure 9. Wind speed distribution at 40 m.

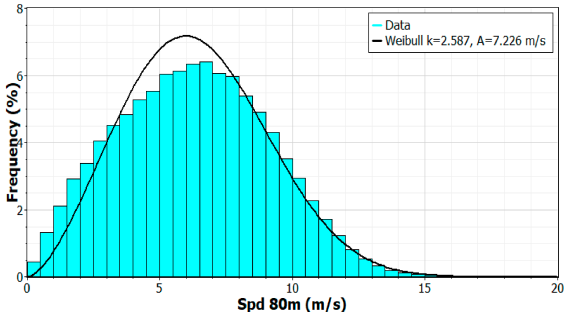


Figure 10. Wind speed distribution at 80 m.

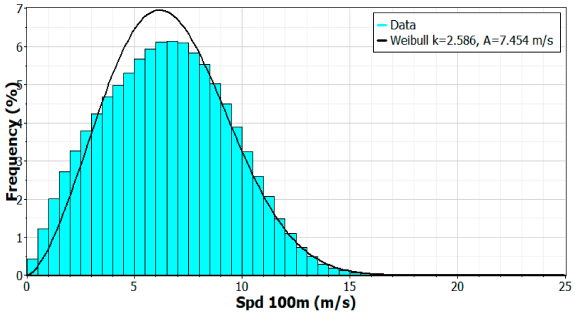


Figure 11. Wind speed distribution at 100 m.

5.3. Cumulative Probability Distribution

Used to estimate the relative of turbine working time above the starting speed, and it reflects the probability of wind speed will be smaller than or equal to a certain value. Figure 12 shows the cumulative distribution at three heights. Table 7 presents two critical wind energy parameters, *k* and *c*, at various altitudes. These characteristics provide essential locational information. The shape parameter stays invariant with altitude since it is independent of wind speed; however, the scale parameter varies with wind speed (altitude) because it is a function on wind speed. It is clear that the speed of the wind at 40 m, 80 m and 100 m heights is more than 4 m/s for 75%, 80% and 81% (Table 7) within a year, respectively. Numerous commercial turbines start operation around 3 to 4 m/s, often 4 m/s, serving as a typical upper limit rather than a universal standard [31]. According to this data, the wind at 40 m, 80 m, and 100 m above ground is more than 5 m/s for 60%, 67%, and 70% of the year, respectively. Thus, it is evident that there is considerable wind potential for wind turbine installation.

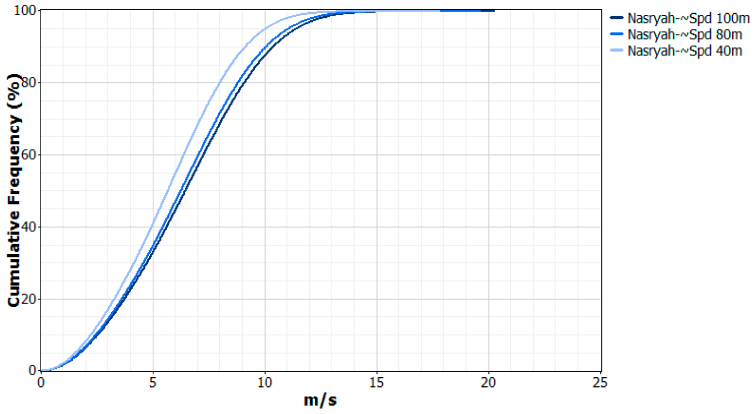


Figure 12. Cumulative distribution for three heights.

Table 7. Weibull parameters at 40 m, 80 m, and 100 m heights.

Height (m)	Weibull Shape k	Weibull Shape c (m/s)	Time Fraction 4 m/s	Time Fraction 5 m/s
40	2.587	6.558	75%	60%
80	2.587	7.226	80%	67%
100	2.586	7.454	81%	70%

5.4. Wind Rose Representation of Wind Direction

When analyzing wind data, predicting the wind's direction is crucial, particularly when deciding where to put wind turbines or wind farms. One useful technique for showing the wind direction during a site study is a wind rose. Wind rose at 40 m, 80 m, and 100 m

for the examined location is shown in Figure 13. The winds are mostly blowing from the northwest. Figure 14 shows the wind rose for each month, revealing the frequency of wind speed patterns across different directions and altitudes (40 m, 80 m, 100 m). The summer months (Jun, Jul, Aug, and Sep) exhibit the highest frequency of wind speed patterns at varying altitudes, indicating that the highest energy levels are typically obtained during this season. In addition, it can be observed that the prevailing wind direction throughout the year is northwesterly for all months of the year and across the different seasons.

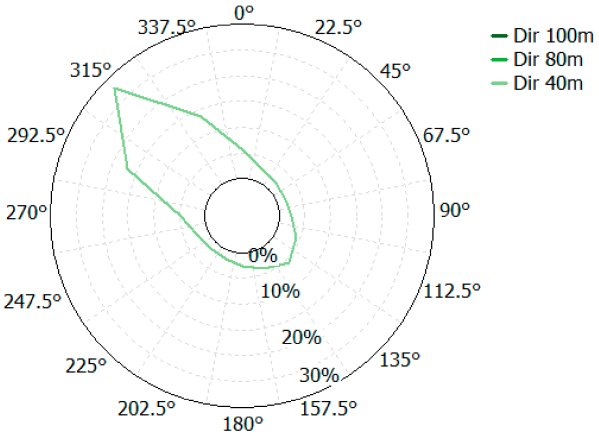


Figure 13. Wind rose at 40 m, 80 m, and 100 m heights.

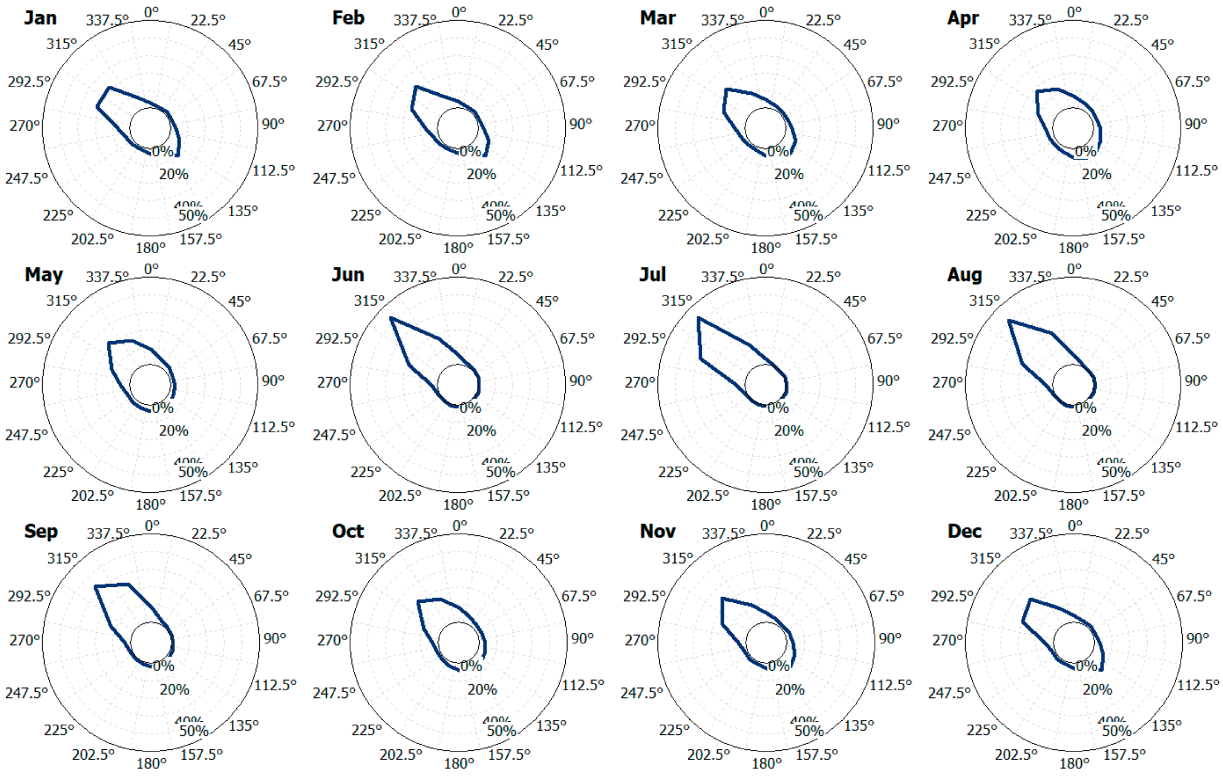


Figure 14. Monthly frequency of speeds vs. directions at 100 m, 80 m, and 40 m heights.

5.5. Wind Power Density

Power density is a key parameter deliver supporting information for evaluating site suitability [27]. Thus, the wind power density at Nasiriya Airport was computed. At 100 m, maximum wind power density varies between 185 W/m^2 in Nov and 525 W/m^2 in Jun. While at 80 m and 40 m heights the maximum wind power density varies between 164 and 478 W/m^2 and between 123 and 357 W/m^2 in Nov to Jun. Figure 15 illustrates that only

months from Jun to Aug have wind power density more than 400 W/m^2 at 100 m height. The results indicate that the Nasiriya Airport possesses fair potential of power density and may be suitable for large-scale wind turbines at 80 m between 6 and 15 km, provided that the proposed installations comply with the ICAO obstacle limitation surface (OLS)and do not affect airport systems. At 40 m above ground, the density of power is around 123 W/m^2 in Nov to 357 W/m^2 in Jun. Months of Mar, May, Jun, July, Aug, and Sep have mean power density greater than 200 W/m^2 (see Table 8).



Figure 15. Hourly mean power density for whole months.

Table 8. Monthly power density at 40 m, 80 m, and 100 m heights.

Month	Jan	Feb	Mar	Apr	May	Jun	Jul	Aug	Sep	Oct	Nov	Dec
Height 100 m												
Min	137	168	178	143	134	291	297	200	142	92	85	116
Max	228	261	331	288	320	525	515	428	338	253	185	203
Height 80 m												
Min	125	153	162	130	122	265	271	182	129	84.3	77.4	106
Max	208	238	302	263	292	478	469	390	308	230	164	184
Height 40 m												
Min	93.1	115	121	97.1	91.5	198	202	136	96.7	63	57.8	79.1
Max	155	178	226	196	218	357	350	291	230	172	123	138

5.6. Turbulence Intensity

Topography causes ambient turbulence and wind turbines cause induced turbulence. Woods, hills, and cliffs provide ambient turbulence. By avoiding key geographical features, ambient turbulence may be reduced. Wake effects generate huge turbulence more than ambient turbulence. Reducing the space will increase the turbulence from neighbor turbines' wakes, suggesting turbine placement restrictions. Turbines in the prevailing direction of the wind should be at least five rotor diameters apart [32]. Wind speed in flat terrain increases logarithmically with altitude, but in the presence of obstacles, the intensity of wind turbulence increases, which leads to high fatigue loads, especially on the yaw system. Obstructions such as buildings may similarly influence the wind profile and should thus be avoided. Figure 16 illustrates the hourly rate of variation throughout the year for the monthly mean wind speed and corresponding turbulence intensity. The monthly variation in turbulence intensity displays high values reaching 0.188 in November. The high turbulence intensity values are mostly seen during daylight hours from 06:00 to 18:00, especially in January, February, March, and October. Figure 16 shows an inverse relationship between wind speed and turbulence intensity associated with surrounding atmospheric disturbances. A decrease in wind speed corresponds to an increase in turbulence intensity, and vice versa.

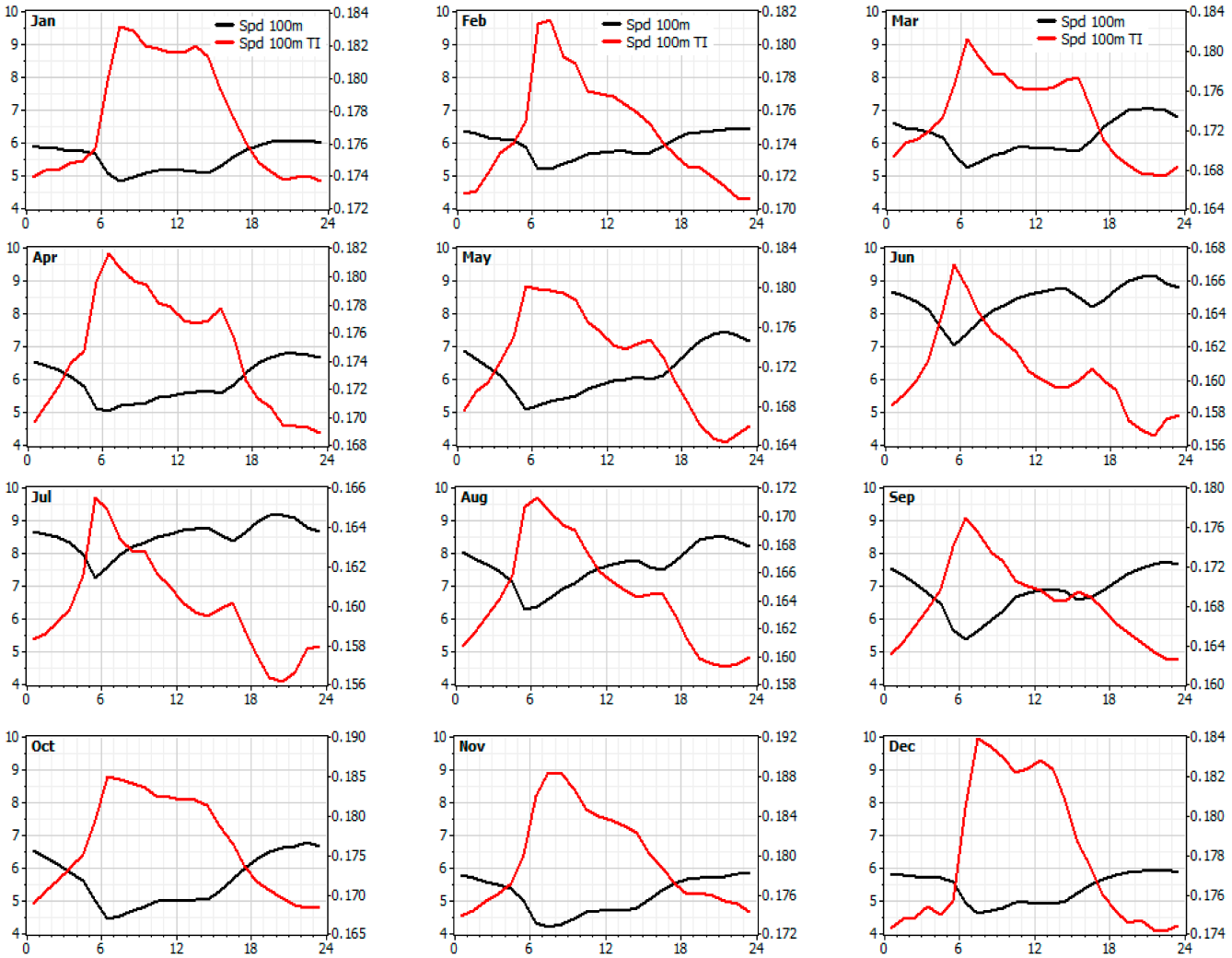


Figure 16. Variation in turbulence intensity with hourly mean wind speed in the study region throughout the study period.

Figure 17 shows the wind flower for the surrounding turbulence intensity values, where there are two turbulence intensities, one in the northeast direction and the other in the southwest direction. It is equal at different altitudes; therefore, these two directions (northwest and southeast) should be taken into account when attempting to build a wind farm on this site.

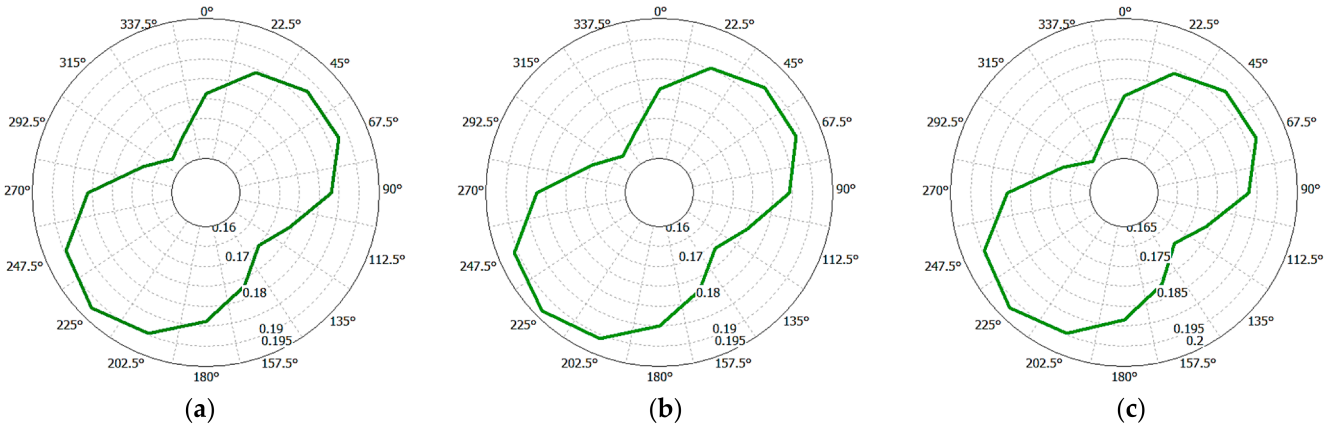


Figure 17. Mean turbulence intensity at (**a**) 100 m, (**b**) 80 m, (**c**) 40 m heights vs. direction sensor at same heights, respectively.

From Table 9, the typical turbulence intensity at 15 m/s is around 0.14 at all measurement heights (40 m, 80 m, and 100 m), according to the turbulence intensity study done using Windographer 4. For this reason, the site is categorized as Turbulence Category A in accordance with IEC 61400-1 (3rd edition). While the appropriate wind turbine Class for the study site can be estimated from Table 1. Since the average wind speed v_{ave} does not reach 7 m/s, the appropriate wind turbine class is the 3rd one (class III).

Table 9. Turbulence intensity (TI) analysis at multiple heights based on IEC 61400-3.

	All Speed Bins			15 m/s Speed Bin			
	Data	**Std.-TI**	**TI-Rep**	**Data**	**Std.-TI**	**TI-Rep**	**Category**
WS_100 m	1,048,563	0.02	0.20	2394	0.001	0.140	A
WS_80 m	1,048,563	0.02	0.20	1548	0.001	0.140	A
WS_40 m	1,048,563	0.02	0.21	312	0.001	0.140	A

5.7. Energy Generation from Wind Turbine

This section of the research compares the energy output of ten wind turbines at various heights from various manufacturers. It should be noted that vertical extrapolation is used to determine the wind speed at various heights (Equation (7)). Table 10 displays each wind turbine's rated output and rotor diameter [33]. Figure 18 shows the power curve for each wind turbine; the turbine has multiple power curves due to the multiplicity of air densities. The cut-in wind speed varies across the examined wind turbine types. The proven 15 kW exhibits the lowest cut-in velocity at 2 m/s. The EWT54_900 and Enercon101 function at a cut-in speed of 2.5 m/s, but the Acciona77/1500, Endurance3120, Nordex117/2400, Vestas100/1.8, and DeWind6_64 m exhibit a cut-in speed of 3 m/s. Mitsubishi92/2.4 and Suzlon52/600 exhibit higher values, both needing 4 m/s to start power production.

Table 10. Characteristics of wind turbine [33].

Turbine Symbol	Wind Energy System	Diameter of the Rotor (m)	Rated Output Power (kW)
a	Acciona77/1500	77	1500
b	Endurance3120	19.2	35
c	Nordex117/2400	117	2400
d	Vestas100/1.8	100	1800
e	EWT54_900	54	900
f	DeWind6_64 m	64	1250
g	Enercon101	101	3050
h	Mitsubishi92/2.4	61.4	1000
i	Proven15	9	15
j	Suzlon52/600	52	600

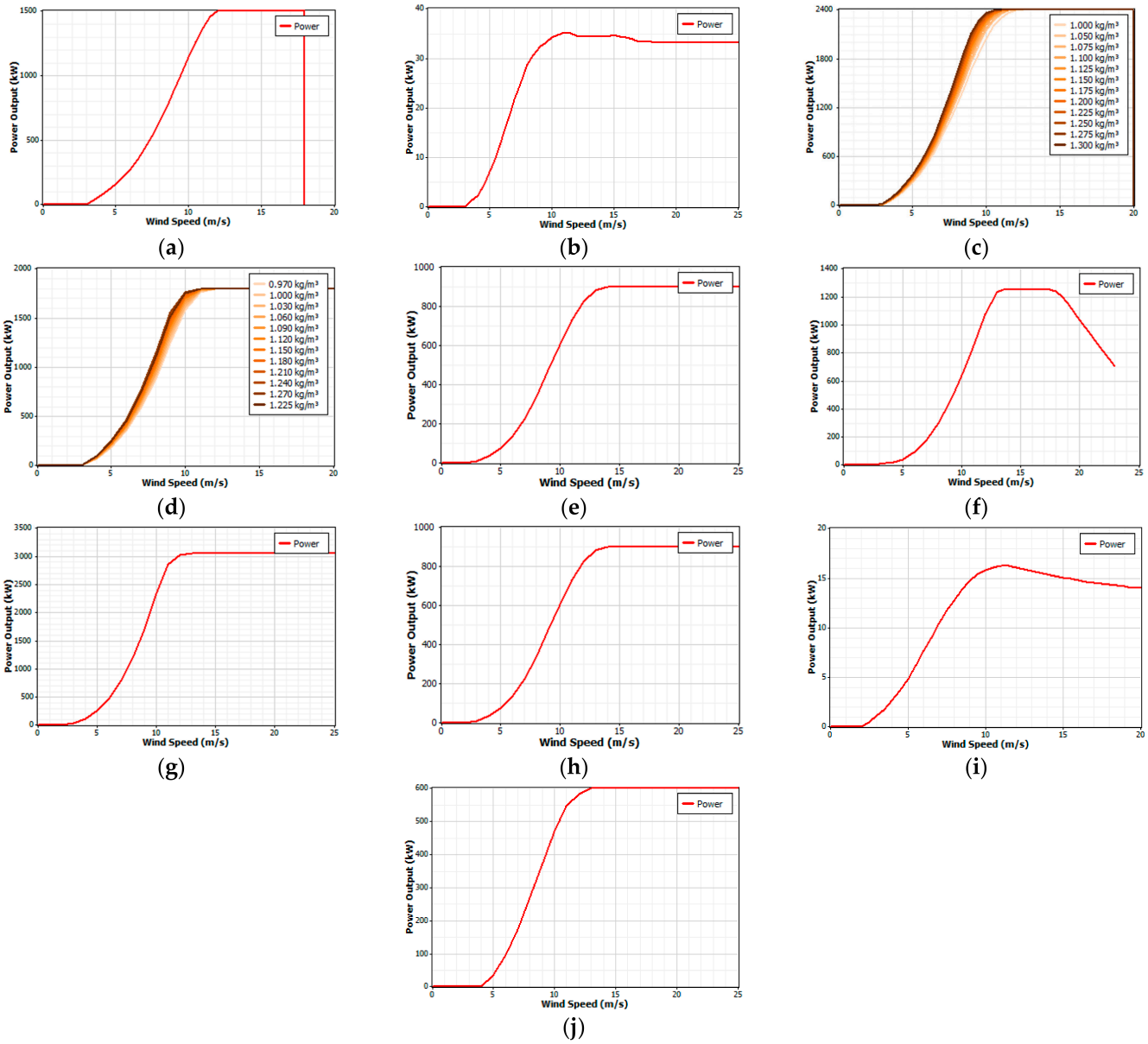


Figure 18. Representative wind turbine systems analyzed in the present study: (**a**) Acciona77/1500 (1.5 MW); (**b**) Endurance3120; (**c**) Nordex117/2400 (2.4 MW); (**d**) Vestas100/1.8 (1.8 MW); (**e**) EWT54_900 (0.9 MW); (**f**) DeWind6_64 m; (**g**) Enercon101; (**h**) Mitsubishi92/2.4 (2.4 MW); (**i**) Proven15; and (**j**) Suzlon52/600 (0.6 MW) [33].

Table 11 presents the hub height wind speed for each turbine. The wind speed at a height of 100 m is measured at 6.4 m/s. Table 12 summarizes the annual mean net energy yield and corresponding capacity factor for each wind turbine model. It indicates that the maximum energy output attained was 7259 MWh/year for the "Nordex N117/2400" at an elevation of 91 m. Table 12 demonstrates that energy generation from the wind turbines Nordex117/2400, Vestas100/1.8, Enercon101 and Mitsubishi92/2.4, making them appropriate for the advancement of wind energy at Nasiriyah Airport. Conversely, we note that the capacity factor ranges between 20% and 35%.

Table 11. Turbine hub height and wind speed value of each turbine model.

Turbine Symbol	Wind Turbine	Hub-Height (m)	Wind Speed (m/s)
a	Acciona77/1500	80	6.2
b	Endurance3120	42.7	5.7
c	Nordex117/2400	91	6.3
d	Vestas100/1.8	95	6.4
e	EWT54_900	50	5.8
f	DeWind6_64 m	65	6.0
g	Enercon101	100	6.4
h	Mitsubishi92/2.4	60	6.0
i	Proven15	25	5.4
j	Suzlon52/600	75	6.1

Table 12. Each wind turbine's average net energy production and turbine capacity factor.

Turbine Symbol	Wind Turbine	Energy Output (MWh/yr)	Capacity Factor (%)
a	Acciona77/1500	3276	25
b	Endurance3120	104	34
c	Nordex117/2400	7259	35
d	Vestas100/1.8	5356	34
e	EWT54_900	1373	17
f	DeWind6_64 m	1551	14
g	Enercon101	6834	26
h	Mitsubishi92/2.4	4209	20
i	Proven15	47	35
j	Suzlon52/600	1254	24

It is advisable to install commercial-grade wind turbines at Nasiriyah Airport to capture wind power for energy production. The Nordex117/2400 and Enercon101 models are optimal selections according to their high-power output and capacity factor, making them suited for extensive wind energy development and electricity generation at Nasiriyah Airport.

6. Conclusions

This study analyzed wind data at different heights to assess the wind energy potential at Nasiriyah Airport, Iraq, using the Weibull probability distribution function. The results showed that the prevailing wind direction is from the northwest, suggesting that any future wind farm development should preferably be oriented in this direction. Turbulence intensity analysis indicated that a Class IIIA wind turbine may be suitable for the site conditions. The mean annual wind speeds were found to be 5.708 m/s, 6.290 m/s, and 6.489 m/s at heights of 40 m, 80 m, and 100 m, respectively. The Weibull distribution demonstrated strong agreement with the observed wind data, confirming its reliability for wind resource assessment in the study area.

Higher wind energy potential was observed during the summer months (June to August), with wind speeds ranging from 6.8 to 7.4 m/s. During this period, the wind power density at 100 m height exceeded 400 W/m^2, indicating favorable conditions for wind energy generation. The analysis of ten wind turbines revealed improved energy production at higher hub heights, with estimated annual energy production exceeding 7000 MWh/year at 100 m height. The maximum annual energy output was estimated at 7259 MWh/year with a capacity factor of approximately 35%, suggesting that the site has promising potential for utility-scale wind energy applications.

Furthermore, turbine placement should consider airport safety regulations, with installations preferably located on the northern and southern sides of the airport away from the runway. In addition, turbines lower than 50 m should be located at least 10 km from the runway, while turbines below 150 m should be placed at a minimum distance of 15 km to support safe airport operations.

Author Contributions: F.A.H. contributed to conceptualization, data curation, formal analysis, and funding acquisition. S.J.H. contributed to funding acquisition, methodology, validation, and writing—review and editing. Q.M.A. contributed to funding acquisition, methodology, investigation, validation, and visualization. R.A.A. contributed to supervision, software, project administration, and writing—review and editing. K.A.-K. contributed to resources, project administration, and writing—original draft preparation. All authors have read and agreed to the published version of the manuscript.

Funding: This research received no external funding.

Institutional Review Board Statement: Not applicable.

Informed Consent Statement: Not applicable.

Data Availability Statement: The data supporting the findings of this study are publicly available in the GitHub (https://github.com/) repository: Nasiriya-Airport (https://github.com/Firas-hadi/Nasiriya-Airport.git, accessed on 21 June 2026).

Acknowledgments: We are deeply grateful to everyone who supported and encouraged us throughout this research journey. Our sincere thanks go to our colleagues and institution for their guidance and resources. We also appreciate the thoughtful feedback from reviewers, which made this work stronger. Above all, we thank our families for their patience, encouragement, and unwavering support.

Conflicts of Interest: The authors declare no conflicts of interest.

Nomenclature

The definition of symbols

Symbol	Description	Unit	Mathematical Representation
v	Wind speed	m/s	$v \in [0, \infty)$
k	Weibull shape parameter	–	$k > 0$
c	Weibull scale parameter	m/s	c > 0
$f\,(v)$	Weibull probability density function	–	
W_p	Wind power density	W/m^2 or kW/m^2	$W_p = \frac{1}{2n}\sum_{i=1}^{n} \rho\, v_i^3$
U	Mean wind speed	m/s	$U \in [0, \infty)$
$\frac{P}{A}$	Wind power density in terms of Weibull distribution function	W/m^2 or kW/m^2	$\frac{1}{2}\rho c^3 \Gamma\left(1 + \frac{3}{k}\right)$
$f(U)$	Cumulative distribution function in Weibull representation	–	$1 - exp\left[-\left(\frac{U}{c}\right)^k\right]$
σ	Standard deviation of wind speed fluctuations	m/s	$\sigma = \sqrt{\frac{1}{N-1}\sum_{i-1}^{N}(U_i - \overline{U})^2}$

Symbol	Description	Unit	Mathematical Representation
U	Mean wind speed	m/s	
U_i	Instantaneous wind speed measurement	m/s	ith wind speed observation
$\overline{U}$	Average wind speed	m/s	
N	Number of wind speed observations	–	Total sample size
Z_{ref}	Reference height above ground level	meter	–
Z	Target (hub) height above ground level	meter	–
α	Wind shear exponent	–	Surface roughness parameter
v_r	Reference wind speed at reference height	m/s	Measured wind speed
TI	Turbulence intensity	– (or %)	$TI = \sigma/U$
I_{ref}	Reference turbulence intensity at a mean wind speed of 15 m/s	–	Ste specific parameter
P_w	Mean wind turbine power output	W or kW	$= \int_0^\infty \boldsymbol{P}(\boldsymbol{U})\boldsymbol{P}(\boldsymbol{U})d\boldsymbol{U}$
$C.F$	Capacity factor	–	$= \frac{\exp[-(v_c/c)^k] - \exp[-(v_r/c)^k]}{(v_r/c)^k - (v_c/c)^k} - \exp[-(v_f/c)^k]$
P_R	Rated power of the wind turbine	kW or MW	Manufacturer rated power

References

1. Yadav, B.K.; Yadav, R.; Jahangiri, M.; Priya, S.S.; Bajracharya, T.R.; Sudhakar, K. Decarbonizing airport using solar and wind farm: A case of Biratnagar, Nepal. *e-Prime-Adv. Electr. Eng. Electron. Energy* **2024**, *8*, 100583. [CrossRef]
2. Raimundo, R.J.; Baltazar, M.E.; Cruz, S.P. Sustainability in the airports ecosystem: A literature review. *Sustainability* **2023**, *15*, 12325. [CrossRef]
3. Ortega Alba, S.; Manana, M. Energy research in airports: A review. *Energies* **2016**, *9*, 349. [CrossRef]
4. de Rubeis, T.; Nardi, I.; Paoletti, D.; Di Leonardo, A.; Ambrosini, D.; Poli, R.; Sfarra, S. Multi-year consumption analysis and innovative energy perspectives: The case study of Leonardo da Vinci International Airport of Rome. *Energy Convers. Manag.* **2016**, *128*, 261–272. [CrossRef]
5. Cuadra, L.; Ocampo-Estrella, I.; Alexandre, E.; Salcedo-Sanz, S. A study on the impact of easements in the deployment of wind farms near airport facilities. *Renew. Energy* **2019**, *135*, 566–588. [CrossRef]
6. Santa, S.L.B.; Ribeiro, J.M.P.; Mazon, G.; Schneider, J.; Barcelos, R.L.; de Andrade, J.B.S.O. A Green Airport model: Proposition based on social and environmental management systems. *Sustain. Cities Soc.* **2020**, *59*, 102160. [CrossRef]
7. Xiang, Y.; Cai, H.; Liu, J.; Zhang, X. Techno-economic design of energy systems for airport electrification: A hydrogen-solar-storage integrated microgrid solution. *Appl. Energy* **2021**, *283*, 116374.
8. Goh, H.H.; Suo, W.; Liang, X.; Zhang, D.; Dai, W.; Kurniawan, T.A.; Goh, K.C. An adaptive energy management strategy for airports to achieve carbon neutrality by 2050 via waste, wind, and solar power. *Front. Energy Res.* **2024**, *12*, 1365650. [CrossRef]
9. Al-Zain, Y.; Bqoor, M.; Albqoor, M.; Ismail, L. Next-Generation Airborne Pathogen Detection: Flashing Ratchet Potential in Action. *Chemosensors* **2025**, *13*, 371. [CrossRef]
10. Mehta, H.; Kanani, P.; Lande, P. Google maps. *Int. J. Comput. Appl.* **2019**, *178*, 41–46. [CrossRef]
11. Hadi, F.A.; Oudah, S.S.; Al-Baldawi, R.A. Pre-feasibility study of hypothetical wind energy project using simulated and measured data. In Proceedings of the 2018 2nd International Conference for Engineering, Technology and Sciences of Al-Kitab (ICETS), Karkuk, Iraq, 4–6 December 2018; pp. 60–65.
12. Guenoupkati, A.; Salami, A.A.; Bokovi, Y.; Koussetou, P.X.; Ouedraogo, S. Estimating mixture hybrid Weibull distribution parameters for wind energy application using Bayesian approach. *Int. J. Renew. Energy Dev.* **2023**, *12*, 902–912. [CrossRef]
13. Sewter, A.; Neill, S.P. The co-location of wind and wave energy at multiple global sites. *Renew. Energy* **2025**, *255*, 123765. [CrossRef]
14. Hou, C.; Xu, Z.; Karnauskas, K.B.; Huang, D.; Lu, H. Detecting and calibrating large biases in global onshore wind power assessment across temporal scales. *Nat. Commun.* **2025**, *16*, 3775. [CrossRef] [PubMed]
15. Londo, N.A.P.; Londo, D.S.L.; Hugo, R.O.; Londo, F.; Salcán, N.S.; Campoverde-Santos, D.K.; Quingatuña, D.; Coello-Cabezas, J. Estimation of Weibull distribution parameters to assess the wind energy potential of high altitude sites in the Andean region of Ecuador. *Results Eng.* **2025**, *27*, 106053. [CrossRef]
16. Alanazi, M.A.; Aloraini, M.; Islam, M.; Alyahya, S.; Khan, S. Wind energy assessment using Weibull distribution with different numerical estimation methods: A case study. *Emerg. Sci. J.* **2023**, *7*, 2260–2278. [CrossRef]
17. Hasan, W.S.; Hassan, A.S.M.; Shukri, M.A. Assessment of wind power potential and economic viability at Al-Hodeidah in Yemen: Supplying local communities with electricity using wind energy. *Energy Rep.* **2024**, *12*, 2981–2996. [CrossRef]
18. Khanjari, A.; Feroz, A.; Archer, C.L. An analytical formulation for turbulence kinetic energy added by wind turbines based on large-eddy simulation. *Wind Energy Sci.* **2025**, *10*, 887–905. [CrossRef]

19. Frech, J.; Saha, K.; Lavin, P.D.; Zhang, H.-M.; Reagan, J.; Fung, B. A new gridded offshore wind profile product for US coasts using machine learning and satellite observations. *Wind Energy Sci. Discuss.* **2024**, *10*, 1077–1099.
20. Li, X.; Liu, C.; Chen, C.; Zhou, F. Fine-Scale Temporal Wind Variability in ERA5 and Its Implications for Wind Stress Calculation. *Remote Sens.* **2025**, *17*, 3068. [CrossRef]
21. Dai, S.; Song, Y.; Zhu, Y.; Ye, M.; Wang, H.; Wen, J.-F. Recalibration of IEC Turbulence Model Based on Field Observations. *J. Mar. Sci. Eng.* **2025**, *13*, 1957. [CrossRef]
22. Donnou, H.E.V.; Akpo, A.B.; Houngue, G.H.; Kounouhewa, B.B. Assessment of IEC normal turbulence model and modelling of the wind turbulence intensity for small wind turbine design in Tropical Area: Case of the coastal region of Benin. *Int. J. Renew. Energy Dev.* **2020**, *9*, 263–286. [CrossRef]
23. Meyer, P.J.; Huhn, M.L.; Gottschall, J. Development of a Load Model Validation Framework Applied to Synthetic Turbulent Wind Field Evaluation. *Energies* **2024**, *17*, 797. [CrossRef]
24. Freudenreich, K.; Argyriadis, K. The load level of modern wind turbines according to IEC 61400-1. *J. Phys. Conf. Ser.* **2007**, *75*, 012075. [CrossRef]
25. Garcia-Ribeiro, D.; Malatesta, V.; Moura, R.C.; Ceron-Munoz, H.D. Assessment of RANS-type turbulence models for CFD simulations of horizontal axis wind turbines at moderate Reynolds numbers. *J. Braz. Soc. Mech. Sci. Eng.* **2023**, *45*, 566. [CrossRef]
26. Chau, T.T.; Nguyen, T.T.H.; Nguyen, L.; Do, T.D. Wind Speed Probability Distribution Based on Adaptive Bandwidth Kernel Density Estimation Model for Wind Farm Application. *Wind Energy* **2025**, *28*, e2970. [CrossRef]
27. Ramli, M.A.; Bouchekara, H.R. Wind Resource Assessment for Potential Wind Turbine Operations in the City of Yanbu, Saudi Arabia. *Energies* **2025**, *18*, 2139. [CrossRef]
28. Criado Risco, J.; Valotta Rodrigues, R.; Friis-Møller, M.; Quick, J.; Mølgaard Pedersen, M.; Réthoré, P.-E. Gradient-based wind farm layout optimization with inclusion and exclusion zones. *Wind Energy Sci.* **2024**, *9*, 585–600. [CrossRef]
29. Salma, V.; Ruiterkamp, R.; Kruijff, M.; Van Paassen, M.; Schmehl, R. Current and expected airspace regulations for airborne wind energy systems. In *Airborne Wind Energy: Advances in Technology Development and Research*; Springer: Berlin/Heidelberg, Germany, 2018; pp. 703–725.
30. Lee, K.-S. A Study on the Obstacles of Domestic Aviation Law. *Korean J. Air Space Law Policy* **2006**, *21*, 97–133.
31. Chioncel, C.P.; Spunei, E.; Tirian, G.-O. Wind Turbines Around Cut-In Speed: Startup Optimization and Behavior Analysis Reported to MPP. *Appl. Sci.* **2025**, *15*, 3026. [CrossRef]
32. Cheng, S.; Elgendi, M.; Lu, F.; Chamorro, L.P. On the wind turbine wake and forest terrain interaction. *Energies* **2021**, *14*, 7204. [CrossRef]
33. Mojtaba, N. Wind resource assessment in Abadan airport in Iran. *Int. J. Renew. Energy Dev.* **2012**, *1*, 87–97. [CrossRef]

Disclaimer/Publisher's Note: The statements, opinions and data contained in all publications are solely those of the individual author(s) and contributor(s) and not of MDPI and/or the editor(s). MDPI and/or the editor(s) disclaim responsibility for any injury to people or property resulting from any ideas, methods, instructions or products referred to in the content.